Journal of Artificial Intelligence
ISSN: 2229-3965 & E-ISSN: 2229-3973, Volume 3, Issue 2, 2012, pp.-56-73
Available online at http://www.bioinfo.in/contents.php?id=71

A REVIEW OF NEURAL SIGNAL PROCESSING PARADIGMS BASED ON PHYSIOLOGICAL MODELS FOR EEG

HARISH KUMAR GARG[1], POONAM GAKHAR KOHLI[2] AND AMIT KUMAR KOHLI[3]

[1,3]ECE Department, Thapar University, Patiala-147004, Punjab, India.
[2]Department of Physiology, Punjab Institute of Medical Sciences, Jalandhar-144001, India.
*Corresponding Author: Email- [1]harishgarg17@gmail.com [2,3]drkohli_iitr@yahoo.co.in

Received: February 07, 2012; Accepted: February 21, 2012

Abstract- The electroencephalogram (EEG) is a non-invasive method of demonstrating cerebral function and it gives a course view of the neural activity. The EEG signal also indicates the electrical activity of the brain, which is highly random in nature. The EEG forward problem deals with the mapping of the current dipoles using the lead field matrix (LFM) of the observation model and finding the potential at an electrode. The hypothetical dipoles or a current distribution inside the head provides scalp potentials. However, the EEG inverse problem deals with the problem of estimating the spatially extended sources of the electroencephalogram from corresponding scalp recordings of the EEG, i.e. for estimating the current distribution within human brain. By introducing dynamical inverse solutions, it is possible to link systematically the temporal aspect of EEG time series modeling with the spatial aspect of the instantaneous inverse solutions. The EEG consists of an underlying background process with superimposed transient nonstationarities such as epileptic spikes (ESs). The detection of ESs in EEG is of particular importance in the diagnosis of epilepsy. The EEG signal is modeled as time-varying autoregressive (TVAR) model. The Kalman filter is used to estimate the parameters of the TVAR model. A threshold function is applied to estimate the EEG to detect epileptic spikes. The EEG is susceptible to various large signal contaminations or artifacts, like baseline wander, power line, muscle activity (EMG), Electrooculogram or eye blinking (EOG), electrocardiogram (ECG), electrode movement and the normal brain background activity (sharp alpha activity or SAA). An independent component analysis (ICA) method and cascade adaptive filter may be used efficiently to remove the artifacts and interferences.
Key words- Nonstationary EEG, epileptic spikes (ES), EEG inverse problem, Kalman filtering (KF), Akaike information criterion (AIC), artifacts.

Citation: Harish Kumar Garg, Poonam Gakhar Kohli and Amit Kumar Kohli (2012) A Review of Neural Signal Processing Paradigms based on Physiological Models for EEG. Journal of Artificial Intelligence, ISSN: 2229-3965 & E-ISSN: 2229-3973, Volume 3, Issue 2, 2012, pp.-56-73.

Introduction

The electroencephalogram (EEG) is a most commonly used instrument for clinical evaluation of human brain activity, discovered by Hans Berger in 1929. The clinical interpretation of bioelectrical signals plays an important role in the diagnosis of human being diseases, in which the important information is frequently carried by small amplitude bioelectric signals. The EEG is a clinical tool used in diagnosis, monitoring and management of neuro physiological disorder related to epilepsy. The epilepsy is characterized by the sudden recurrent and transient disturbances of mental functions and movement of body due to excessive electrical discharge in the brain. During the seizures (ictal activity), the EEG is characterized by high amplitude synchronized periodic waveforms due to epilepsy. These high amplitude synchronized periodic waveforms reflect abnormal discharge of a large group of neurons. Between, before and after seizures (interictal activity), the EEG might contain occasional epileptiform transient waveforms. The Epileptiform activity (EFA) refers to the waves recorded in the interictal activity, which can be divided in spikes, sharp waves, spike-and-slow-wave complex, and multiple spike-and-slow-wave complexes. A signal modelling approach is used to detect these ESs in EEG recordings.

The aspects of the brain that are the fundamental to this model include neuron, thalamus and cortex. The neuron is the most fundamental unit of the brain and nervous system. These cells communicate to each other via connections from axons to den-

drites across a gap called a synapse. The impulses propagate through these via electrochemical gradients (action potentials) The pulses arrive at the dendrites, and are carried down to the cell body (soma). They then travel down the axon hillock to the axonal tree, where they are then imparted to other neurons. However, there are different types of neurons in the brain. The pyramidal cells are of particular importance, comprising 90% of the cerebral cortex and also play an essential part in the most neuronal circuits. There are also inhibitory cells that inhibit signals by chemical means, the action of these are highly localised.

The physiology of the brain may be represented by a model. The physiological model has neuronal population of the cortex and the thalamus. The cerebral cortex comprises the greatest volume of the brain, but it is the structure that lies closest to the recording electrodes of an EEG. The cortex is the outermost layer of the brain; it is the main contributor to the scalp potentials as it is the closest to the scalp and also the site of termination of many of the electrical signals that arrive to the brain. The cortex receives most of the sensory information from the thalamus. With a relative thickness of 2-4 mm, it is often treated in its unfolded state as a 2D sheet with a total length of 1 m. The thalamus is the main gating station for all sensory input received from the peripheral nervous system (except smell) and relays this information to other parts of the brain, namely the cortex. It also receives feedback from the cortex and forms closed corticothalamic loops. The thalamus is broken up into two main divisions, the relay nuclei, which function to transmit the signals to the cortex, and the reticular nucleus, which has an inhibitory effect on these signals. The sensory information from external stimuli comes through the thalamus, which then transmitted to other structures in the brain. A series of electrical pulses travel to the thalamus and are then sent primarily to the cerebral cortex, where they are further processed. This leads to the interactions in the form of circuits or loops between populations within the thalamus to the cortex and vice versa.

Here a two-dimensional model is considered that specifically incorporates the dynamics of neuron somas, synapses and axonal propagation. The cortex consists of a large number of macrocolumns, each containing around 105 neurons in a volume of 1 mm2 area by 1 mm2 thickness. The cortex model is a two-dimensional continuous area of macrocolumns. The mean-field continuum approach uses a set of coupled differential equations in time and space to describe the excitatory, inhibitory soma potentials within the cortex and the time-evolution of postsynaptic potentials (PSPs). The localization of neural brain sources based on EEG uses scalp potential data to infer the location of underlying neural activity. This procedure entails with

i)Modeling of the brain electrical activity

ii)Modeling of the head volume conduction process for linking the neural electrical activity to EEG recordings, and

iii)Reconstructing the brain electrical activity from recorded EEG data (measured scalp potentials)

The first two modelling steps serve to solve the so-called EEG forward problem, which describes the distribution of electric potentials for the given source locations, orientations and signals. The third modelling step serves to solve the inverse of the previous ones; thereby it is commonly referred to as the EEG inverse problem solution. A model of brain electrical activity (in short “source model”) is composed of bioelectric units distributed within the entire brain volume or over specific brain surfaces or confined to a few brain locations. A single source unit is often modelled as a current dipole, which well approximates the synchronized synaptic currents at a columnar level. When confined to the cerebral cortex, the orientation of the current dipoles can be either free or constrained to be perpendicular to the cortical surface. Linking the source model to the physical electromagnetic signals measurable at the sensor locations on the scalp (forward model) require the construction of a volume conductor model that explains the propagation of the currents throughout the human head in terms of geometry and conductivity of this medium. The modelling errors produced by the differences between the actual head and the volume conductor model affect the accuracy of the EEG forward and also the inverse problem solution, as the observed scalp potentials are determined not only by the location and strength of the neural generators, but also by the geometry and the conductive properties of the head. The modelling errors include differences in actual head and model shape, skull thickness, and electrical conductivities of the head tissues.

The forward problem estimates the scalp potential i.e. EEG signal. The scalp potential is represented by time varying AR model. The parameters of the model may be estimated by Kalman filter. The use of time-varying AR model enhances spikes. The EEG inverse problem is applied to the task of localising the source of an epileptic spike from a clinical EEG data set. The inverse problem reconstructs EEG source by mapping the voltage back on scalp, and also finds the current dipole position on the scalp (true location of source). Then, the filter may be used to estimate dynamic neural activity from EEG signals for the cases of linear and nonlinear models having either time-invariant or time-varying parameters. A Kalman filtering approach using physiological models may be used for linear model, in which both spatial and temporal dynamics are used to estimate dynamic neural activity from EEG signals. The best performance in terms of estimation is achieved with a nonlinear model with time-varying parameters.

The EEG is a set of data measured by electrodes placed on the scalp, and is always influenced by artifacts. There are several types of noises and artifacts in the EEG signal. The occurrence of artifacts in EEG recording obscures the underlying processes and makes EEG analysis difficult. The scalp EEG is severely contaminated by low frequency artifacts (baseline wander) of high amplitude produced by movement of the patients and varying electrode-skin impedance. The strong signals from A/C power supplies can corrupt EEG data during transfer from scalp electrodes to recording device. The additive artifacts EMG, EOG and ECG are caused by activity in different muscle groups like neck and facial muscles, the reorientation of the retinocorneal dipole; and when an electrode is placed near a blood vessel, it causes pulse or heart beat. The recordings are therefore low-pass filtered to remove low-frequency artifacts (usually between 0.5 and 1 Hz) and also high-pass filtered to remove high-frequency artifacts (usually between 35 and 70 Hz). However, most EEG machines have configurable noise cancellation options already built-in.

In the next section, we describe the EEG model, followed by Section III, which describes mathematical physiological model to evaluate the inverse problem. Section IV describes the physiology and

detection of Epileptiform activity. Finally, Section V represents a review of EEG artifacts contaminating our EEG dataset, and approaches taken in an attempt to remove these artifacts.

EEG Source model

Reconstruction of EEG source is a technique that reconstructs the electrical currents within the brain that gives rise to recordable potential fields at the scalp. The EEG source reconstruction is also known as source localization. In nature, the human brain is the most complex system. The neurons of brain relay information by electrical pulses, known as action potentials. The electromagnetic fields can be detected outside the head produced by electrical activity of large assemblies of neurons.

The electrical fields can be observed as weak voltages by electrodes attached to the skin and connected to differential amplifiers, giving rise to the electroencephalogram (Nunez, 1981). The EEG time-series contains detailed information on brain activity. The EEG source localization allows high temporal (milliseconds) resolution, but relatively low spatial (centimetres) resolution. The inverse problem is non-unique due to small number of spatial measurements (≤256) and volume conduction effects. To make the problem tractable, the priori assumptions (mathematical, anatomical and physiological) are imposed on the source and head model. Solution of the EEG inverse problem has two main classes. The first type is ''parametric'' method (also known as ''equivalent current dipole'' approach), in which the sources are modelled by a relatively small number of focal sources at locations to be estimated from the data. The second type is ''linear distributed'' approaches (also known as ''imaging'' or ''current density reconstruction'' methods), in which the sources are modelled by a dense set of dipoles (3-D grid of dipoles) distributed at fixed locations (voxels) throughout the head volume. The various techniques described for non parametric methods are low resolution electrical tomography methods (LORETA), standardized low resolution brain electromagnetic tomography (sLORETA), variable resolution electrical tomography methods (VARETA), quadratic regularization and spatial regularization (S-MAP), spatio-temporal regularization (ST-MAP), Backus-Gilbert, local autoregressive average (LAURA), shrinking LORETA FOCUSS (SLF), standardized shrinking LORETA FOCUSS (SSLOFO) and adaptive standardized LORETA FOCUSS (ALF). The techniques for parametric methods are beam forming techniques, brain electric source analysis (BESA), subspace techniques such as multiple-signal classification (MUSIC), first principal vector (FINES), simulated annealing (SA) and computational intelligence algorithms.

The EEG potential sources are commonly modelled by current dipoles, forming a time-dependent distribution over all electrically active parts of the brain. To which extent, the field of a single dipole can be detected by a given pair of electrodes will depend not only on the position, but also on the direction of the dipole. Moreover, each pair of electrodes will record a superposition of the fields of all current dipoles that have suitable positions and directions. If detailed information about the activity at particular sites of the cortex or within deeper structures is required, it is usually necessary to attach electrodes directly to the brain tissues in question, i.e. to resort to invasive methods. As an alternative to invasive approaches, one could try to estimate the time-dependent distribution of source currents from the EEG time-series data by appropriate numerical procedures; this task represents the inverse problem of EEG generation. Distributed source model presents a highly ill-posed inverse problem, particularly due to mismatch between the small number of measurements and the number of states to be estimated. One of the approaches for the inverse problem of EEG generation is LORETA (Pascual-Marqui et al., 1994; Strobach et al., 1994). This method is instantaneous, i.e. it is applied repeatedly to the data recorded at each point of time, without taking the information into account, which is encoded in the temporal order of the available data. It ignores a huge amount of the temporal order information. The temporal order of the data directly reflects the dynamics of the sources, while instantaneous methods play no role to give the temporal information of the source.

Recently various methods have been developed, which are applied to solve the inverse problem of EEG generation by exploiting temporal information (Galka et al., 1994a; Galka et al., 1994b). A linear model, which is a stochastic variant of a standard damped wave equation, is suggested for modelling of EEG data in (Barton et al., 2009). A linear state space (LSS) model describes the generation of the EEG from the primary current density vector field.

For the inverse direction, i.e. for the estimation of the primary current density from the EEG, a generalised variant of Kalman filtering can be employed. After fitting the LSS model to the data, estimates for the time-dependent primary current density can be obtained. The discretized state space model can be formulated in a different way; this will allow us to add moving-average (MA) terms to the dynamics, which leads to a more powerful model. The modified state space representation offers a very efficient implementation of this generalised predictive model.

Another model "state space generalised autoregressive conditional heteroscedasticity GARCH/SSGARCH" is introduced in (Yamashita et al., 2004) for the state-adaptive covariance within Kalman filter, but it is unable to estimate additional model parameters within the maximum-likelihood framework. The improved procedure, such as nonlinear maximization of likelihood is given in (Ary et al., 1981). In this method, the direct comparison with LORETA via information criteria such as Akaike information criterion (AIC) and Bayesian information criterion (BIC) demonstrate that the dynamical model offers a much superior description of the data, as compared to LORETA. The AIC minimization step selects appropriate model parameters and noise covariances, which results in a well tuned filter as indicated by the reconstructed current densities and diagnostics. This shows that the likelihood maximization is effective for filter tuning, but tuning still requires an appropriate process model to be chosen. The process model is a telegrapher's equation, which contains a resonance, whose properties are examined.

In (Ary et al., 1981), the space- and time-invariant models for data description are more suitable in combination with AIC minimization criterion. A number of potentially rewarding directions are identified, which focused on selecting an appropriate process model, variation of model parameters on the need for spatiotemporal and on handling the problem's high dimensionality.

The application of Kalman filtering to source localization is examined through a detailed study of the KF based inverse solution described in (Barton et al., 2009). A modified KF algorithm reduces the high dimensionality of this problem by reformulating it as a coupled set of low-dimensional KFs running in parallel. A single

telegrapher's equation is used to model the global source dynamics; the likelihood maximization to estimate a small number of model parameters and noise parameters. This technique offers improved source localization over existing instantaneous solutions (e.g., LORETA).

EEG Forward Problem Formulations

The EEG forward problem deals with the estimate of the potential $g(r, r_{dip_i}, j_{e_i})$ at an electrode. A single dipole has position vector r with dipole moment j_{e_i} (with magnitude j and orientation e_i), positioned at r_{dip_i}. The Poisson's equation is used to find the potentials V on the scalp for different configurations of r_{dip_i} and j_{e_i}. For multiple dipole sources, the electrode potential would be

$$y(r) = \sum_i g(r, r_{dip_i}, j_{e_i}) \quad (1)$$

Assuming the principle of superposition, this can be rewritten as

$$\sum_i g(r, r_{dip_i})(j_{ix}, j_{iy}, j_{iz})^T = \sum_i g(r, r_{dip_i}) j_i e_i \quad (2)$$

where $g(r, r_{dip_i})$ has three components corresponding to the cartesian x, y, z directions, $J_i = (j_{ix}, j_{iy}, j_{iz})$ is a vector consisting of the three dipole magnitude components, $(.)^T$ denotes the transpose of a vector, $J_i = \|J_i\|$ is the magnitude of its dipole and $e_i = J_i / \|J_i\|$ is its dipole orientation. In practice, one calculates the potential between an electrode and the reference (which can be another electrode or an average reference). For N_e electrodes and P dipoles, it is clear that

$$\vec{y} = \begin{bmatrix} y(r_1) \\ . \\ . \\ . \\ y(r_{N_e}) \end{bmatrix}_{N_e \times 1} = \begin{bmatrix} g(r_1, r_{dip_1}) & . & . & . & g(r_1, r_{dip_P}) \\ . & . & & & . \\ . & & . & & . \\ . & & & . & . \\ g(r_{N_e}, r_{dip_1}) & . & . & . & g(r_{N_e}, r_{dip_P}) \end{bmatrix}_{N_e \times P} \begin{bmatrix} j_1 e_1 \\ . \\ . \\ . \\ j_P e_P \end{bmatrix}_{P \times 1} \quad (3)$$

$$\vec{y} = \begin{bmatrix} y(r_1) \\ . \\ . \\ . \\ y(r_{Ne}) \end{bmatrix}_{N_e \times 1} = \vec{G}(\{r_l, r_{dip_i}\})_{N_e \times P} \begin{bmatrix} j_1 e_1 \\ . \\ . \\ . \\ j_P e_P \end{bmatrix}_{P \times 1} \quad (4)$$

where $i = 1,2,...,P$ and $l = 1,2,...,N_e$. Each row of the gain matrix $\vec{G}(\{r_l, r_{dip_i}\})$ is often referred to as the lead-field, and it describes the current flow for a given electrode through each dipole position. For N_e electrodes, P dipoles and $k = 1,2,...,N_k$ discrete time samples, it can be shown that

$$\vec{Y}_{N_e \times N_k} = \begin{bmatrix} y(r_1,1) & . & . & . & y(r_1, N_k) \\ . & . & & & . \\ . & & . & & . \\ . & & & . & . \\ y(r_{N_e},1) & . & . & . & y(r_{N_e}, N_k) \end{bmatrix}_{N_e \times N_k}$$
$$= \vec{G}(\{r_l, r_{dip_i}\})_{N_e \times P} \begin{bmatrix} j_{1,1} e_1 & . & . & . & j_{1,N_k} e_1 \\ . & . & & & . \\ . & & . & & . \\ . & & & . & . \\ j_{p,1} e_p & . & . & . & j_{p,N_k} e_P \end{bmatrix}_{P \times N_k} \quad (5)$$

Where, $\vec{Y}$ is the matrix of data measurements at different times $y(r,t)$. In the above formulation, it is assumed that both the magnitude and orientation of the dipoles are unknown. However, based on the fact that apical dendrites producing the measured field are oriented normal to the surface, dipoles are often constrained to have such an orientation. In this case, only the magnitude of the dipoles will vary and the formulation in (3) can therefore be re-written as

$$\vec{y} = \begin{bmatrix} g(r_1, r_{dip_1}) e_1 & . & . & . & g(r_1, r_{dip_P}) e_P \\ . & . & & & . \\ . & & . & & . \\ . & & & . & . \\ g(r_{N_e}, r_{dip_i}) e_1 & . & . & . & g(r_{N_e}, r_{dip_P}) e_P \end{bmatrix}_{N_e \times p} \begin{bmatrix} j_1 \\ . \\ . \\ . \\ j_P \end{bmatrix}_{p \times 1} \quad (6)$$

From (5)

$$\vec{Y}^{(1)} = \vec{G}^{(1)}(\{r_l, r_{dip_i}, e_i\})_{N_e \times p} \begin{bmatrix} j_{1,1} & . & . & . & j_{1,N_k} \\ . & . & & & . \\ . & & . & & . \\ . & & & . & . \\ j_{p,1} & . & . & . & j_{p,N_k} \end{bmatrix}_{p \times N_k} \quad (7)$$

$$\vec{Y}^{(1)}_{N_e \times N_k} = \vec{G}^{(1)}(\{r_l, r_{dip_i}, e_i\})_{N_e \times p} \vec{J}^{(1)}_{p \times N_k} \quad (8)$$

where, $\vec{J}^{(1)}$ is now a matrix of dipole magnitudes at different time instants. Generally, a noise or perturbation matrix $\vec{\varepsilon}^{(1)}$ is added to the system such that the recorded data matrix $\vec{Y}^{(1)}$ is composed of

$$\vec{Y}^{(1)} = \vec{G}^{(1)}\vec{J}^{(1)} + \vec{\varepsilon}^{(1)} \tag{9}$$

Under this notation, the gain matrix $\vec{G}^{(1)}$ is calculated in the forward problem. $\vec{G}^{(1)}$ is obtained by solving the forward problem for each dipole location and orientation. The data is corrupted by additive measurement noise $\vec{\varepsilon}^{(1)}$. If the term $N_k = 1$ in Eq. (5), then Eq. (5) is equal to Eq. (3).

EEG Inverse Problem Formulations

The inverse problem consists of finding estimates of the dipole magnitude matrix, given the electrode positions and scalp readings $\vec{Y}^{(2)}$. The EEG inverse problem defines a continuous current vector field $\vec{J}^{(2)}(s,t)$, where s and t denote space and time, respectively. The solution space is discretized into N_v grid points (voxels) $s_v = 1,2,...,N_v$, restricted to the cortical gray matter of the brain, where the majority of the EEG signals are generated (Nunez and Srinivasan, 2006). Time is discretized into N_k points, $k = 1,2,...,N_k$. Discretized points are indicated by s_v and k here. At each voxel, the state vector is

$$j^{(2)}(s_v,k) = [j_x^{(2)}(s_v,k), j_y^{(2)}(s_v,k), j_z^{(2)}(s_v,k)]^T \tag{10}$$

The global state vector for the entire system has dimension $N_J \times 1 = 3N_v \times 1$, and it follows that

$$\vec{J}^{(2)}(s,k) = [j^{(2)}(1,k)^T, ..., j^{(2)}(N_v,k)^T]^T \tag{11}$$

The EEG signal that is recorded on the scalp at N_e electrode sites produces the current at each electrode. If $y(l,k)$ is the EEG voltage at a single electrode, where l is an electrode label ($l = 1,2,...,N_e$); the N_e-dimensional column vector composed of all the electric potentials at all available electrodes shall be denoted by

$$\vec{Y}(k) = [y(1,k), ..., y(N_e,k)]^T \tag{12}$$

Here, voltages refer to average reference (the average voltage is subtracted from each channel). The EEG signal is estimated by exploiting temporal information that relates to the current vectors by

$$\vec{Y}^{(2)}(k) = \vec{G}^{(2)}\vec{J}^{(2)}(s,k) + \vec{\varepsilon}^{(2)}(k) \tag{13}$$

where the $N_e \times N_J$ matrix $\vec{G}$, often referred to as the lead field matrix (LFM) of the observation model, and also maps the current vectors to voltages at the scalp electrodes. In basic representation, an EEG measures the electric signals from the scalp with international 10-20 electrode placing system. In (Barton et al., 2009), the LFM is approximated for the 10-20 system (the 10-20 system defines a number of electrodes locations by dividing the head into 10% and 20% interval using the nasion and the inion as landmark for the front to back direction and preaurical points for the side to side direction) by solving the vector Laplace equation for a three-shell spherical head model via the boundary element method.

The dimensions of $\vec{Y}^{(2)}(k)$ and $\vec{J}^{(2)}(s,k)$ are $N_e \times 1$ and $N_J \times 1$. The term $\vec{\varepsilon}^{(2)}(k)$ is a $N_e \times 1$ dimensional vector of observational noise, which is assumed to be white Gaussian noise (WGN) with zero mean and covariance matrix $\vec{C}_\varepsilon$, and uncorrelated between all pairs of sensors, with equal variance σ_ε^2 at every electrode, so

$$\vec{C}_\varepsilon = \sigma_\varepsilon^2 I_{N_e} \tag{14}$$

where, I_{N_e} is the $N_e \times N_e$ identity matrix.

Equation (13) cannot be inverted directly due to the large ratio of solution points to measurements. Hence, the inverse problem can only be solved by introducing additional constraints. The KF-based source localization technique is proposed in (Galka et al., 1994b). Key features of this algorithm are the following: the process model is a space and time-invariant telegrapher's equation and a spatial whitening transformation is used to reduce its computational burden. Subsequently, the filter is tuned using likelihood maximization.

Mathematical Physiological Model

The incorporation of linear and nonlinear physiological models into inverse solution framework can provide a better description of the system dynamics. To observe brain activity and EEG, a compact model is used. This is based on the mean field formulation of the brain. This model is described by a single second order delay differential equation, which has only one explicit variable, the corticocortical activity. The model can be linearized near steady states, captures the essential features of activities such as corticocortical propagation and delayed feedbacks via extracortical pathways and external stimuli. Furthermore, a nonlinear model is derived from compact model in the vicinity of steady states. The

linear models of first and second order with time invariant parameters are employed in (Robinson et al., 1997; Robinson and Kim, 2007; Giraldo et al., 2010).

Cortical Modeling based on Physiology

The first feature incorporated is the neural response to the cell-body potential. An excitatory neuron emits pulses (i.e., fires) at a mean rate q_e that is determined by the potentials generated in the dendritic tree by synaptic inputs of thousands of other neurons. Threshold potentials, above which high firing rates occur, are not identical for all the neurons, but have centrally peaked distribution. The local mean firing rate Q_e averaged over many neurons replaces q_e. The mean dendritic potential V_e is introduced. The Q_e is measured in units of the maximum value possible (250-1000 s^{-1} per neuron), and potential V_e is measured in units of the characteristic standard deviation of the threshold distribution. Similar considerations apply for inhibitory neurons, denoted by subscript i. The mean firing rate Q_e of excitatory $(a = e)$ and inhibitory $(a = i)$ neurons are nonlinearly related to mean potential V_a measured relative to the resting level, by $Q_a(r,t) = S[V_a(r,t)]$, where S is the sigmoidal function that increases from 0 to $Q_{\max}$ as V_a increases from $-\infty$ to $+\infty$. It follows that

$$Q_a = S(V_a) = \frac{Q_{\max}}{1 + e^{-(V_a - \theta)/\sigma'}} \tag{15}$$

where $Q_{\max}$ is the maximum firing rate, θ is the mean firing threshold and $\sigma'\pi/\sqrt{3}$ is the standard deviation of the threshold distribution in the neural population. The θ and σ' are measured in mV.

The signals arriving at neurons of type a, stimulate neurotransmitter release at synapses. This is followed by propagation of voltage changes along dendrites, with cable properties that tend to spread out the temporal profile of the signals (a form of low-pass filtering). The total cell body potential V_a can thus be written as

$$V_a(r,t) = \sum_b V_{ab}(r,t) \tag{16}$$

where the subscript b on the components V_{ab} distinguishes the different combinations of afferent neural type and synaptic receptor, $r = (x, y)$ denotes the spatial coordinates, and t is the time. The weighted average over the receptor time constants to yield effective values that will change when and if different receptors dominate the dynamics in different brain states. This can be written by

$$D_a(t)V_a(r,t) = \sum_b N_{ab}S_{ab}\phi_b(r, t - \tau_{ab}) \tag{17}$$

$$D_a(t) = \left[\frac{1}{\alpha\beta}\frac{d^2}{dt^2} + \left(\frac{1}{\alpha} + \frac{1}{\beta}\right)\frac{d}{dt} + 1\right] \tag{18}$$

where $D_a = D_{\alpha\beta}$ encapsulates the overall time constants, in which α and β are the mean decay and rise rates, respectively, of the cell-body potential produced by an impulse at dendritic synapses, and $\beta = 4\alpha$. The use of a single form of D_a corresponds to the approximation that the mean dendritic dynamics can be described by a single pair of time constants. On the right-hand side of Eq. (17), substitute, the value of $V_a(r,t)$ from Eq. (16) and then, replace $V_{ab}(r,t)$ by $N_{ab}S_{ab}\phi_b(r, t - \tau_{ab})$, where N_{ab} is the mean number of synapses from neurons of type $b = e, i, s$ to type $a = e, i$; and S_{ab} is the mean time-integrated strength of soma response per incoming spike, and $\phi_b(r, t - \tau_{ab})$ is the mean spike arrival rate from neurons b, allowing for a time delay τ_{ab} due to anatomic separations. The quantities a and b corresponds to the excitatory (e), inhibitory (i), reticular thalamic (r) and specific relay (s) population and to external stimuli (n). The only nonzero values of τ_{ab} in our model are $\tau_{es} = \tau_{se} = \tau_{re} = t_0/2$, which correspond to cortico-thalamic and thalamocortical propagation times. The time t_0 can be related to the characteristic loop length R and mean

axonal velocity V by $t_0 = R/V$. Each part of the corticothalamic system gives rise to neural pulses, whose values averaged over short scales form a field $\phi_a(r,t)$ in this model that propagates at a velocity v_a. To a good approximation, a obeys a damped wave equation whose source of pulses is

$$D_a(r,t)\phi_a(r,t) = S[V_a(r,t)] \tag{19}$$

$$D_a(r,t) = \left(\frac{1}{\gamma_a^2}\frac{\partial^2}{\partial t^2} + \frac{2}{\gamma_a}\frac{\partial}{\partial t} + 1 - r_a^2\nabla^2\right) \tag{20}$$

The potential V_a obeys the following differential equation:

$$D_{\alpha\beta}V_a(r,t) = v_{ae}\phi_e(r,t) + v_{ai}\phi_i(r,t) + v_{as}\phi_s(r,t-t_0/2) \tag{21}$$

The ϕ_{ei} is the contributions from other cortical neurons, and inputs ϕ_s from thalamic relay nuclei, delayed by a time $t_0/2$ required for signals to propagate from thalamus to cortex. The corticothalamic system it produces a field ϕ_a of pulses that travels at a velocity v_a (e.g., for excitary neurons $v_e = 10ms^{-1}$) and obeys a damped wave equation

$$\left(\frac{1}{\gamma_a^2}\frac{\partial^2}{\partial t^2} + \frac{2}{\gamma_a}\frac{\partial}{\partial t} + 1 - r_a^2\nabla^2\right)\phi_a(r,t) = Q_a(r,t) \tag{22}$$

$$\left(\frac{1}{\gamma_a^2}\frac{\partial^2}{\partial t^2} + \frac{2}{\gamma_a}\frac{\partial}{\partial t} + 1 - r_a^2\nabla^2\right)\phi_a(r,t) = S[V_a(r,t)] \tag{23}$$

where $\gamma_a = v_a/r_a$ is the temporal damping rate of pulse in axon a (mean decay rate), and r_a is the mean range of axons a (assumed to have an approximately exponentially decreasing distribution at large ranges). The γ_a, v_a and r_a are measured in units s^{-1}, ms^{-1} and m. If intracortical connectivities are proportional to the numbers of synapses involved, $V_i = V_e$ and $Q_i = Q_e$ which lets us concentrate on excitatory quantities. The smallness of r_i also lets us set $\gamma_i = \infty$ and $r_i = 0$. The model incorporates corticothalamic connectivities and thalamic nonlinearities. The latter relay external stimuli ϕ_n to the cortex as well as corticothalamic feedback. The cell-body potentials then satisfy

$$D_{\alpha\beta}V_c(r,t) = v_{ce}\phi_e(r,t-t_0/2) + v_{cs}\phi_s(r,t) + v_{cr}\phi_r(r,t) + v_{cn}\phi_n(r,t) \tag{24}$$

where, there is a delay $t_0/2$ for signals to travel from cortex to thalamus or back, $c = r,s, v_{cc} = v_{rn} = 0,$ and $\phi_c(r,t) = S[V_c(r,t)]$, applies because the small size of the thalamic nuclei enables us to assume γ_c large $(\gamma_c = \infty)$ and $r_c = 0$ for $c = r,s$ in Eq. (23). The ϕ_a and v_{aa} are measured in units s^{-1} and mVs. It is assumed that α and β are large compared to $\partial/\partial t$, therefore, it can be written as $D_{\alpha\beta} = 1$ in Eq. (21). Use as the approximations $V_i = V_e$, $\gamma_a = \infty$ and $r_a = 0$ results in a single nonlinear equation for $V_e(r,t)$. Solving this transcendental equation for $S(V_e)$ we obtain the formal solution in terms of a function f that only depends on $\phi_e(r,t)$, $\phi_e(r,t-t_0)$ and $\phi_n(r,t-t_0/2)$. It leads to

$$S[V_e(r,t)] = f\left(\phi_e(r,t),\phi_e(r,t-t_0),\phi_n(r,t-t_0/2)\right) \tag{25}$$

Substituting Eq. (25) in Eq. (23), we get a single time-delayed differential equation with one variable ϕ_e.

$$\frac{1}{\gamma_e^2}\frac{\partial^2\phi_e(r,t)}{\partial t^2} + \frac{2}{\gamma_e}\frac{\partial\phi_e(r,t)}{\partial t} - r_e^2\nabla^2\phi_e(r,t) = -\phi_e(r,t) + f\left(\phi_e(r,t),\phi_e(r,t-t_0),\phi_n(r,t-t_0/2)\right) \tag{26}$$

This compact model requires only ϕ_e describing the brain activity (Robinson et al., 1997; Robinson and Kim, 2007), which implies that the brain dynamics can be studied in a reduced space under certain conditions. The Eq. (26) depends on only three quantities with apparent physiological meanings. The term $\phi_e(r,t)$ represents activities due to nearby neurons, $\phi_e(r,t-t_0)$ denotes delayed feedbacks via extracorticocortical loop, and the external stimulus is $\phi_n(r,t-t_0/2)$. Here, the delay time of the external stimulus is $t_0/2$, since the stimulus is relayed to cortex via

ties, c_2 parametrizes corticothalamic feedbacks, and c_3 parametrizes a delayed external stimulus that can be considered as random noise in many cases. The term μ_a represents the densities of synapses associated with stimuli. The solutions of linear dynamics model is well defined in the stable region only and diverge in the unstable region. Some nonlinear properties such as limit cycle and bifurcations are observed. To treat these nonlinear properties, the nonlinear dynamics model is considered. In nonlinear dynamics model, Eq. (25) is expanded for cubic terms (Robinson and Kim, 2007). Expanding the left-hand side of Eq. (27) up to cubic terms, Eq. (33) becomes

$$q_e(t) + \eta_{e2} q_e^2(t) + \eta_{e3} q_e^3(t) = \mu_{ee}\bar{\phi}_e(t) + \mu_{ei} q_e(t) + \mu_{es} q_s(t - t_0/2) \tag{41}$$

$$\eta_{e2} = \frac{2Q_e^* - Q_{\max}}{Q_e^*(Q_{\max} - Q_e^*)} \tag{42}$$

$$\eta_{e3} = \frac{2[3(Q_e^*)^2 - 3Q_e^* Q_{\max} + Q_{\max}^2]^2}{Q_e^*(Q_{\max} - Q_e^*)} \tag{43}$$

We may replace q_s on the right-hand side of Eq. (41) with the linearized solution $q_s^{(1)}$ obtained from Eqs. (33)-(35), and its solution is generally too complex. If $\gamma_e \succ\succ 1/t_0$ and $q_e \approx \bar{\phi}_e$ at a steady state. The Eq. (41) is further approximated by replacing all the q_e on the left-side with $\bar{\phi}_c$. Subsequently, the equation (26) gives explicit form as

$$\frac{\partial^2 \chi_e(R,\tau)}{\partial \tau^2} + 2\frac{\partial \chi_e(R,\tau)}{\partial \tau} - \nabla_R^2 \chi_e(R,\tau) = \begin{pmatrix} h_1\chi_e(R,\tau) + h_2\chi_e(R,\tau-\tau_0) + \varepsilon_2\chi_e^2(R,\tau) + \\ \varepsilon_3\chi_e^3(R,\tau) + h_3\chi_n(R,\tau-\tau_0/2) \end{pmatrix} \tag{44}$$

where, the coefficients h_d and ε_d are related to physiological model and $d = 1,2,3...n$. Right-hand side of Equation (44) depends only on the intracortical activity (first, third, and fourth terms), the delayed corticothalamic feedback (second term), and the delayed external input (last term).

$$h_1 = -1 + \frac{1-\mu_{ee}}{\mu_{ei}} \tag{45}$$

$$h_2 = \frac{-\mu_{es}(\mu_{se} + \mu_{sr}\mu_{re})}{\mu_{ei}(1-\mu_{sr}\mu_{rs})} \tag{46}$$

$$h_3 = \frac{-\mu_{es}\mu_{sn}}{\mu_{ei}(1-\mu_{sr}\mu_{rs})} \tag{47}$$

$$\varepsilon_2 = \eta_{e2}/\mu_{ei} \tag{48}$$

$$\varepsilon_3 = \eta_{e3}/\mu_{ei} \tag{49}$$

where $\chi_e(R,\tau)$ represents corticocortical activities with strength c_1 due to nearby neurons, $\chi_e(R,\tau-\tau_0)$ denotes delayed feedbacks via extracorticocortical loop with strength c_2, and the external stimulus (random noise) with strength c_3 is $\chi_n(R,\tau-\tau_0/2)$. Based on the abovementioned physiological background, (Robinson et al., 1997; Robinson and Kim, 2007; Galka et al., 2008; Giraldo et al., 2010) have presented the mathematical modelling of compact model.

Spatiotemporal Modeling based on Physiology

The spatiotemporal (process model) describes the system dynamics of the inverse problem, which give rise to the evolution of the current vectors. For this task, the following telegrapher's equation is proposed in (Barton et al., 2009).

$$\frac{\partial^2 j^{(3)}(s,t)}{\partial t^2} + 2\zeta\omega_n \frac{\partial j^{(3)}(s,t)}{\partial t} + \omega_n^2 j(s,t) = b\nabla^2 j^{(3)}(s,t) + \hat{\eta}^{(3)}(s,t) \tag{50}$$

where ω_n is the natural frequency, ζ is the fractional damping coefficient, b is the wave velocity squared, and $\hat{\eta}^{(3)}(s,t)$ is a dynamical (process) noise term. This equation is selected for several reasons: 1) it is the continuous form of the discrete model used here and in (Barton et al., 2009) it contains an explicit temporal resonance, which is a key feature of EEG data; 3) it allows physically meaningful parameters to be determined through the estimation step; and 4) used as mean-field modelling (Galka et al., 1994a), an equivalent equation successfully described the spatiotemporal propagation of neuronal activity. The model defines a continuous current vector field $\vec{J}^{(3)}(s,t)$, where s and t denote space and time, respectively. The solution space is discretized into N_{v_3} grid points s_{v_3}, $v_3 = 1,...,N_{v_3}$. Time is discretized into N_{k_3} points t_{k_3}, $k_3 = 1,...,N_{k_3}$. Discretized points are indicated by r_{v_3} and t_{k_3} here. To implement a KF, Eq. (50) is discretized with respect to space and time to give

$$j^{(3)}(v_3,k_3) = A_{L1} j^{(3)}(v_3,k_3-1) + A_{L2} j^{(3)}(v_3,k_3-2) + B_{L1}[LJ^{(3)}(k_3-1)]_v + \hat{\eta}^{(3)}{}_L(v_3,k_3) \tag{51}$$

at each voxel, where **L** is a discrete 3-D spatial Laplacian operator of dimensions $N_{J^{(3)}} \times N_{J^{(3)}}$ that arises from the discretization of the second spatial derivative in Eq. (50) and is defined as

a half pathway. The linear dynamics model is derived from the compact model Eq. (26) in the vicinity of a steady state (Robinson and Kim, 2007). Assuming that the system is spatially homogenous and $\phi_c(t) = S[V_c(t)]$.

Substitute $D_{\alpha\beta} = 1$, $a = e$, in Eq. (21), which gives

$$V_e(t) = v_{ee}\phi_e(t) + v_{ei}S[V_e(t)] + v_{es}S[V_s(t - t_0/2)] \tag{27}$$

Then, substitute $D_{\alpha\beta} = 1$, $c = r, v_{cc} = v_{rn} = 0,$ in Eq. (24), which gives

$$V_r(t) = v_{re}\phi_e(t - t_0/2) + v_{rs}S[V_s(t)] + v_{cc}\phi_r(t) + v_{rn}\phi_n(t) \tag{28}$$

Substitute $v_{cc}\phi_r(t) = v_{rn}\phi_n(t) = 0$ in Eq. (28)

$$V_r(t) = v_{re}\phi_e(t - t_0/2) + v_{rs}S[V_s(t)] \tag{29}$$

Similarly, substitute $D_{\alpha\beta} = 1$, $c = s, v_{cc} = v_{rn} = 0,$ in Eq. (24), which gives

$$V_s(t) = v_{se}\phi_e(t - t_0/2) + v_{cc}\phi_c(t) + v_{sr}S[V_r(t)] + v_{sn}\phi_n(t) \tag{30}$$

Substitute $v_{cc}\phi_c(t) = 0$ in Eq. (30), such that

$$V_s(t) = v_{se}\phi_e(t - t_0/2) + v_{sr}S[V_r(t)] + v_{sn}\phi_n(t) \tag{31}$$

Since dynamical behaviours near steady state are of most interest, let $Q_a = S(V_a)$, $q_a = Q_a - Q_a^*$, and $\bar{\phi}_a = \phi_a - \phi_a^*$, where $Q_a^* = S(V_a^*)$ and ϕ_a^* are the steady-state values, and simplify the inverse sigmoidal function on the left-hand side of Eqs. (27), (29) and (31) using

$$V_a = S^{-1}(Q_a) = S^{-1}(Q_a^*) + \frac{\sigma'}{Q_a^*(1 - Q_a^*/Q_{\max})} q_a + O(q_a^2) \tag{32}$$

This gives

$$q_e^{(1)}(t) = \mu_{ee}\bar{\phi}_e(t) + \mu_{ei}q_e^{(1)}(t) + \mu_{es}q_s^{(1)}(t - t_0/2) \tag{33}$$

$$q_r^{(1)}(t) = \mu_{re}\bar{\phi}_e(t - t_0/2) + \mu_{rs}q_s^{(1)}(t) \tag{34}$$

$$q_s^{(1)}(t) = \mu_{se}\bar{\phi}_e(t - t_0/2) + \mu_{sr}q_r^{(1)}(t) + \mu_{sn}\bar{\phi}_n(t) \tag{35}$$

where $\mu_{ab} = (v_{ab}/\sigma')[Q_a^*(1 - Q_a^*/Q_{\max})]$ and $q_a^{(1)}$ denotes the approximated value of q_a considering linear terms only. Eliminating $q_s^{(1)}$ and $q_r^{(1)}$ from Eqs. (33) to (35), which gives

$$q_e^{(1)}(t) = \frac{\mu_{ee}}{1 - \mu_{ei}}\bar{\phi}_e(t) + \frac{\mu_{es}(\mu_{se} + \mu_{sr}\mu_{re})}{(1 - \mu_{ei})(1 - \mu_{sr}\mu_{rs})}\bar{\phi}_e(t - t_0) + \frac{\mu_{es}\mu_{sn}}{(1 - \mu_{ei})(1 - \mu_{sr}\mu_{rs})}\bar{\phi}_n(t - t_0/2) \tag{36}$$

Under local activity approximation, $\phi_a(r,t) = S[V_a(r,t)]$, equations (27) to (31) can be solved numerically to predict the response to specified incoming signals ϕ_n in terms of the 16 quantities $t_0, \alpha, \beta, \gamma_e, r_e, Q_{\max}, \theta, \sigma',$ and $N_{ab}S_{ab}$ (this product is also termed v_{ab} below, and we treat eight of these as nonzero and independent on the assumption of random cortical connectivity, which implies $N_{ib} = N_{eb}$ for all b). If the variables $\phi_a/Q_{\max}, v_{ab}/Q_{\max}\sigma', t/t_0, V_a/\sigma'$, and r/r_e are used in place of the dimensional forms, one finds that the solutions depend only on these dimensionless forms, lowering the essential dimensionality of parameter space to 11. This reflects scaling properties under variation of the maximum firing rate, strength of interconnection, time scale, voltage scale, and length scale, respectively. Substituting Eq. (36) into the right-hand side of Eq. (26), finally give the linearized equation

$$\frac{\partial^2\chi_e(R,\tau)}{\partial\tau^2} + 2\frac{\partial\chi_e(R,\tau)}{\partial\tau} - \nabla_R^2\chi_e(R,\tau) = \left(c_1\chi_e(R,\tau) + c_2\chi_e(R,\tau - \tau_0) + c_3\chi_n(R,\tau - \tau_0/2)\right) \tag{37}$$

Where $\tau = \gamma_e t$ is the dimensionless time unit, $\chi_a = \bar{\phi}_a/Q_{\max}$ is a dimensionless field, and $R = r/r_e$ is a dimensionless spatial vector so that $\nabla_R^2 = r_e^2\nabla^2$ is a dimensionless Laplacian, and the coefficients are

$$c_1 = -1 + \frac{\mu_{ee}}{1 - \mu_{ei}} \tag{38}$$

$$c_2 = \frac{\mu_{es}(\mu_{se} + \mu_{sr}\mu_{re})}{(1 - \mu_{ei})(1 - \mu_{sr}\mu_{rs})} \tag{39}$$

$$c_3 = \frac{\mu_{es}\mu_{sn}}{(1 - \mu_{ei})(1 - \mu_{sr}\mu_{rs})} \tag{40}$$

The first term on right-hand side of Eq. (37) represents rapid corticocortical feedbacks, while the second term represents feedback via extracortical pathways delayed by a time τ_0. We therefore argue that c_1 parametrizes the strength of corticocortical activi-

$$L = \left(I_{N_{v_3}} - \frac{N}{6} \right) \otimes I_3 \tag{52}$$

where $\otimes$ indicates Kronecker multiplication, $I_{N_{v_3}}$ denotes the N_{v_3}-dimensional identity matrix and N is neighbourhood matrix of the voxel set, i.e. a $N_{v_3} \times N_{v_3}$ with element $N(v_3, v_3') = 1$, if v_3' is immediately adjacent to v_3 (maximum of six neighbours per voxel in a 3-D rectangular grid) and $N(v_3, v_3') = 0$, otherwise. The $[J^{(3)}]_{v_3}$ operator selects the column vector composed of the three elements of $J^{(3)}$ that correspond to grid point v_3. Restricting attention to classes of process models (Galka et al., 1994a) in which the local current components in each voxel are approximated as behaving independently of each other and only interacting with the corresponding current vectors in neighbouring voxels, gives the following local parameter matrices in Eq. (51)

$$A_{L1} = a_1 I_3; A_{L2} = a_2 I_3; B_{L1} = b_1 I_3 \tag{53}$$

From the discretization of Eq. (50), the model parameters in Eq. (53), assumed to be space- and time-invariant, are

$$a_1 = \frac{2 - (\omega_n \Delta t)^2}{1 + \zeta \omega_n \Delta t} \tag{54}$$

$$a_2 = \frac{\zeta \omega_n \Delta t - 1}{1 + \zeta \omega_n \Delta t} \tag{55}$$

$$b_1 = -\frac{6b(\Delta t)^2}{(\Delta x)^2 (1 + \zeta \omega_n \Delta t)} \tag{56}$$

where Δt and Δx are the time step and voxel size (assuming cubic voxels). From Eq. (51), we write the global process model as a second-order multivariate AR model

$$J^{(3)}(k_3) = A_{G1}^{(3)} J^{(3)}(k_3 - 1) + A_{G2}^{(3)} J^{(3)}(k_3 - 2) + \eta_G^{(3)}(k_3) \tag{57}$$

where the $N_{J^{(3)}} \times N_{J^{(3)}}$ global parameter matrices are

$$A_{G1}^{(3)} = a_1 I_{NJ^{(3)}} + b_1 L; A_{G2}^{(3)} = a_2 I_{NJ^{(3)}} \tag{58}$$

The $N_{J^{(3)}}$-dimensional vector $\eta_G^{(3)}(k_3)$ is a dynamical noise term that is assumed white, Gaussian, and unbiased, with covariance matrix $C_{\eta_G^{(3)}}$. The decomposition of this high-dimensional problem into a set of coupled low-dimensional, voxel-centered, local filtering problems requires this dynamical noise covariance matrix to be diagonal. However, for the process noise, assumption of a diagonal covariance matrix is typically not justified due to nonvanishing instantaneous correlations between neighbouring voxels. So, to diagonalize this matrix, a switch to a transformed (Laplacianized) state space $\tilde{J}^{(3)}(k_3)$ was proposed (Galka et al., 1994a), where

$$\tilde{J}^{(3)}(k_3) = L J^{(3)}(k_3) \tag{59}$$

Assuming that the same form of dynamics govern the Laplacian of $J^{(3)}$, the process model is

$$\tilde{j}^{(3)}(k_3) = A_{G1}^{(3)} \tilde{J}^{(3)}(k_3 - 1) + A_{G2}^{(3)} \tilde{J}^{(3)}(k_3 - 2) + \tilde{\eta}_G^{(3)}(k_3) \tag{60}$$

As a result of this transformation, the dynamical noise covariance matrix $C_{\tilde{\eta}_G^3}$ is closer to diagonal; since applying the Laplacian operator L to the state vector $J^{(3)}$ reduces spatial correlations between neighbouring voxels through (second order) spatial differentiation. Assuming the process noise covariance $\sigma^2_{\tilde{\eta}^{(3)}}$ to be fixed in space and time, the covariance matrix is

$$C_{\tilde{\eta}_G^{(3)}} = \sigma^2_{\tilde{\eta}^{(3)}} I_{NJ^{(3)}} \tag{61}$$

We can rearrange Eq. (60) to obtain

$$J^{(3)}(k_3) = L^{-1} A_{G1}^{(3)} L J^{(3)}(k_3 - 1) + L^{-1} A_{G2}^{(3)} L J^{(3)}(k_3 - 2) + L^{-1} \tilde{\eta}_G^{(3)}(k_3) \tag{62}$$

By equating the process noise term in (62) with the one in (57), we find

$$\eta_G^{(3)}(k_3) = L^{-1} \tilde{\eta}_G^{(3)}(k_3),$$

which yields the process noise covariance matrix in the original space

$$C_{\eta_G^{(3)}} = L^{-1} E(\tilde{\eta}^{(3)} \tilde{\eta}^{(3)T})(L^{-1})^T = \sigma^2_{\tilde{\eta}^{(3)}} (L^T L)^{-1} \tag{63}$$

This state space transformation is called "spatial whitening," and allows decomposition of the filtering problem. From now on, we will operate in this Laplacianized state space by replacing $J(k_3)$ with $\tilde{J}(k_3)$ and $C_{\eta_G^{(3)}}$ with $C_{\tilde{\eta}_G^{(3)}}$. To obtain actual current densities and covariance's, we simply apply the inverse of the spatial whitening transformation; as seen shortly, this step requires one-off inversion of a very large $(\approx 10^4 \times 10^4)$ matrix.

Physiology and Detection of Epileptiform Activity

A. Basic

Electroencephalography (EEG) is the recording of electrical activity along the scalp produced by the firing of neurons within the brain. In clinical contexts, the EEG refers to the recording of the brain's spontaneous electrical activity over a short period of time, usually 20-40 minutes, as recorded from multiple electrodes

placed on the scalp. The EEG plays a decisive role in epilepsy research and treatment. The measured activity changes in EEG depend on the brain status (epilepsy, anesthesia, sleep, coma, encephalopathies, and brain death). A typical adult human EEG signal is about 10μV to 100 μV in amplitude when measured from the scalp, and it is about 10-20 mV when measured from subdural electrodes. The 10-20 EEG measuring system is more practical for its simplicity of use and for the bigger spacing between electrodes, which reduces the possibility of inter electrode interference.

In the 10-20 EEG measuring system, each channel location has a label and/or number to identify its sub-cranial lobe and hemispherical location, where "FP" is the Front-Polar or prefrontal lobe, "F" is Frontal lobe, "T" is Temporal lobe, "C" is Central lobe, "P" is Parietal lobe, and "O" is Occipital lobe. There are two important reference landmarks known as nasion, which is in the front of the head (point between the forehead and nose) and inion, which is located at the back of the skull. To simplify and standardize electrode placement, caps are used, which have a maximum number of openings to place as much electrodes as needed. Since an EEG voltage signal represents a difference between the voltages at two electrodes, the display of the EEG for the reading encephalographer may be set up in one of several ways. The representation of the EEG channels is referred to as a montage.

- **Bipolar montage**

Each channel (i.e., waveform) represents the difference between two adjacent electrodes. The entire montage consists of a series of these channels. For example, the channel "Fp1-F3" represents the difference in voltage between the Fp1 electrode and the F3 electrode. The next channel in the montage, "F3-C3," represents the voltage difference between F3 and C3, and so on through the entire array of electrodes.

- **Referential montage**

Each channel represents the difference between a certain electrode and a designated reference electrode. There is no standard position for this reference; it is however at a different position than the "recording" electrodes. Midline positions are often used because they do not amplify the signal in one hemisphere vs. the other. Another popular reference is "linked ears", which is a physical or mathematical average of electrodes attached to either earlobes or mastoids.

- **Average reference montage**

The outputs of all of the amplifiers are summed and averaged, and this averaged signal is used as the common reference for each channel.

- **Laplacian montage**

Each channel represents the difference between an electrode and a weighted average of the surrounding electrodes.

B. Types of EEG activity

The EEG activity can be divided into different groups, of which some can be labeled normal and some are considered abnormal, or pathological (Indicative of disease). The signal picked up by EEG electrodes can have many different characteristics and labeled as normal, depending on for sleep stage or age. Some frequency-based categories of EEG are described in Table 1. The rhythmic activity within certain frequency bands is found to have biological significance, or associated with certain regions of the scalp.

Table1- Properties of some common EEG rhythms

Name	Frequency limits	Location	Properties
Delta	0.5 - 3.5 Hz	Widespread	Occur in infants and during deep sleep or anesthesia
Theta	3.5 - 7.5 Hz	Mainly in parietal and temporal lobes	Most prominent in small children and during drowsiness or sleep.
Alpha	7.5 - 13 Hz	Rear half of the head	Occur during awake and resting state, high amplitude when eyes closed. Mostly sinusoidal shape.
Beta	above 13 Hz	Most common in frontal and central regions	Often divided in two sub-bands, of which the higher frequencies appear during tension and intense activation of the CNS and the lower are attenuated during mental activity.

Most of the cerebral activity is traditionally thought to be found in the range 1-20 Hz, but recent research suggests that important information can be found in the extremely low frequencies that most EEG amplifiers filter away. The first four frequency bands are not overlapping and cover the whole EEG spectrum, even though the higher frequencies of the Beta band are today usually named Gama rhythms.

The above-mentioned types of activity are "continuous" in the sense that they describe more or less rhythmic activity that goes on for some time, until they are changed by some change in mental state or sleep stage. Many other types are intermittent, meaning that one kind of activity is interrupted by sudden outbursts of other kind of activity. In the seizure case, one type of activity (seizures) can also be superimposed on another (e.g. burst suppression).

The EEG is also used clinically to diagnose coma and encephalopathy conditions as well as to monitor anaesthesia. Most EEG is nowadays digitally sampled between 256 and 512 Hz, although higher frequencies are used sometimes for research purposes.

As opposed to scalp EEG, the Electrocorticography (ECoG) is typically recorded at higher sampling rates, since higher frequencies are better revealed in subdural signals.

C. Epilepsy: A Synopsis

Epilepsy is a chronic neurological disease manifested by abnormal electric discharges in the brain leading to seizures. It affects people of all ages, although it is predominantly a paediatric disorder, with the mean age of epilepsy onset defined in the range between 8 and 10 years. Epilepsy is considered as one of the most common neurological disorders affecting 3 million people in the United States alone.

According to Centres for Disease Control and Prevention, one out of 100 adults has active epilepsy. According to the World Health Organization, it is estimated that 50 million people worldwide have epilepsy, especially children and adolescents, with millions more that go unreported in poor and developing countries. It is estimated that 30% of the epileptic population has poor response to medication, and around 10% undergo surgical intervention [Epilepsy Foundation of America 2008]. Although congenital factors, head traumas and vascular diseases are considered risk

factors, the etiology of epilepsy is unknown for approximately three fourth of all cases. Patient with epilepsy are initially treated with anticonvulsant medication; but in difficult clinical cases, surgery becomes the only alternative for them.

D. Seizures

Brain discharges lasting more than a few seconds usually represent ictal activity (called a seizure) rather than EFA. During a seizure, the EEG clearly shows high activity in most channels, often manifested with much higher frequencies and amplitudes. Frequency and amplitude increase during the seizure or ictal state.

Seizures are the result of abnormal synchronization of groups of neurons, and may or may not give rise to clinical symptoms (symptoms that are easily noticed in the clinic). The type of symptoms depends on the affected part of the brain. If it is a motor area of the brain, then the result can be wild and uncontrollable motion of the body. On the other hand, if it is a sensory area in the brain that is affected, the result may be that the person experiences e.g. visual flashing or unpleasant odors. There may also be sub-clinical seizures that do not cause any detectable symptoms, but are present in the EEG. The seizure is concentrated to the left part of the rear of the brain. The high frequency noise in P4 and T6 is probably due to that the baby was lying with the right side down. Burst-suppression is one of several indicators of severe pathology in the electroencephalogram signal that may occur after brain damage, caused by e.g. asphyxia (insufficient oxygen and nutrient supply) around the time of birth. Certain characteristics of this pattern can provide clinicians with important information about the prognosis of the patient.

As opposed to MRI, CT, PET and SPECT, EEG is a relative inexpensive technology to estimate locations of tumours and epileptic foci in the brain. By reading EEG, experts can find specific patterns, which are indicative of seizure activity. If these patterns consistently repeat in specific electrodes (or channels), then the approximate location of the seizure focus is expected to be in a region enclosing these electrodes. Therefore, the EEG provides a simple way of roughly locating the seizure focus.

With time, procedures to study epilepsy have become more sophisticated and, when necessitated, invasive. For example, part of the pre-surgical evaluation of persons with refractory seizures is the implantation of electrode arrays, which are placed in the cortex of the brain called ECoG. The placement of these arrays coincides with the location, where the seizure focus was suspected by using scalp EEG. The ECoG is considered in clinical practice, the golden standard for locating epileptogenic zones due to its high spatial resolution and lower degrees of noise than the scalp EEG, whose recordings are attenuated due to high scalp inductivity. The treatment options for intractable seizures are limited to resorting the focal resections of abnormal brain tissue, when the epileptogenic region can be accurately defined; a critical task that may require intracranial EEG recordings of seizures to define their onset and region of involvement. More recently, an alternative treatment option has evolved, where chronic intracranial implants apply electrical stimuli directly to the brain surface with the ultimate aim of preventing or aborting seizures. The implants continuously record the EEG activity and apply the stimuli when seizures are detected or are presumed to be imminent.

Usually, signs of the seizure are first observed in specific channels, called “channels that initiate the seizure”, electrode pairs FP1-F7, F7-T3, T3-T5, F8-T4, and T4- T6 initiate the seizure. It has been recently found that these channels are closer to seizure focus or tumour and have much lower coherence than the remaining channels. During pre-surgical evaluation, an electrode grid is usually implanted in the brain of patients for a better localization of the seizure focus. Patients are then put in an observation room until it is deemed that sufficient data containing interictal spikes or seizures is collected. On occasions, this process may last for more than a week.

Then, the patient is sent to the operation room for surgery. But before that, an EEG expert has to visually scan the EEG to find the interictal spikes and seizures, if any. Considering that EEG recording sessions can last for days, reviewing such EEG data can be an exhausting process, besides that it is prone to subjective assessment. However, the detection of seizures during monitoring is crucial for the surgery outcome, since the grid electrodes that initiate the seizure are consequently used to pinpoint the seizure focus more accurately. For that reason, methods for the automated detection of interictal spikes and seizures can serve as valuable tools for the scrutiny of EEG data in a more objective and computationally efficient manner.

E. Interictal Spikes

Interictal spikes are spikes recorded in the time between seizures, while the subject is not having any seizures. Their detection is critical in locating the seizure focus. Interictal spikes usually occur in neighbouring electrodes (spatio-temporal context), consisting on raising and falling amplitude and duration. Medical experts and neuroscientists have established several criteria as necessary conditions to declare the existence of an interictal spike, their detection, and extraction.

F. Epileptiform Activity

Epileptiform activity (EFA) is a term used in EEG to describe waves that are clearly distinguishable from the background activity and are similar to the waves found in EEG from epileptic subjects. The EFA refers to the waves recorded in the interictal activity (the time between seizures), but not during the seizure itself. The EFA can be divided in spikes, sharp waves, spike-and-slow-wave complex, and multiple spike-and-slow-wave complexes. The distinctions are as follows:

- A Sharp wave is a transient distinguishable from EEG background which lasts 70 to 200 milliseconds.
- A Spike is a sharp wave with duration of 20 to 70 milliseconds.
- A Spike-and-slow-wave complex is a spike followed by a slow wave, whereas the later has usually higher amplitude.
- Multiple spike-and-slow-wave complex is a concatenation of spike-and-slow- wave complexes.

In practice, however, it is more important to distinguish them from the background activity than to detect their morphological distinctions. A signal modelling approach is used to detect ESs in EEG recordings. This method is unsupervised, and can be divided into two steps. The first step is a pre-processing step whose main goal is to pre-emphasize the ESs. In the analysis of non-stationary EEG, the interest is often to estimate the time-varying spectral properties of the signal. A traditional approach to this is the spec-

trogram method, which is based on Fourier transformation. The disadvantages of this method are the implicit assumption of stationarity within each segment and poor time/frequency resolution. A better approach is to use parametric spectral analysis methods based on e.g. time-varying autoregressive moving average (ARMA) modelling. The EEG signal is first modelled as an output of time-varying autoregressive model (TVAR). The TVAR parameters are estimated with a Kalman Filter (KF) algorithm. The tracking lag can be avoided using Kalman smoother algorithm. This is the main advantage of the Kalman smoother algorithm compared to other adaptive algorithms. In the second step, ESs are identified by the output of the filter, compared to a threshold. More specifically, a threshold function is applied in the estimated EEG to detect the ESs. To our knowledge, several spike detection algorithms rely on a simple voltage threshold with little or without preprocessing. Simple thresholding has proved to be attractive for the real-time implementations because of its computational simplicity.

Mathematical model of spike detection

I. Pre-emphasis step: Kalman filter

The Kalman filter is a set of mathematical equations that provides an efficient computational (recursive) means to estimate the state of a process, in a way that minimizes the mean of squared error.

The EEG signal is recorded on the scalp at N_e electrodes. The EEG single electrode records the voltage $y(l,t)$, where l is the electrode label; the N_e - dimensional column vector composed of all the electric potentials at all available electrodes. The observation vector containing the scalp voltages at all EEG channels is given as

$$\vec{Y}^{(4)}(t) = [y(1,t),....,y(N_e,t)]^T_{N_e \times 1} \quad (64)$$

and the EEG signal is estimated by

$$[\vec{Y}^{(4)}(t)]_{N_e \times 1} = \vec{G}_{N_e \times N_j}[\vec{J}^{(4)}(t)]_{N_j \times 1} + [\vec{\varepsilon}^{(4)}(t)]_{N_e \times 1} \quad (65)$$

The model defines a continuous current vector field $\vec{J}^{(4)}(t)$, where t denotes the time. The EEG dynamics is estimated using TVAR model of order p given by

$$\vec{J}^{(4)}(t) = A\vec{J}^{(4)}(t-1) + \vec{\eta}^{(4)}(t) \quad (66)$$

where the dimensions of $\vec{J}^{(4)}(t)$ and $\eta^{(4)}(t)$ are $N_j \times 1$. $\eta^{(4)}(t)$ denotes the dynamic noise, which is assumed to be white Gaussian noise with zero mean and covariance matrix $C_\eta = E(\eta^{(4)}\eta^{(4)T})$. When fitting such models to given data, $\eta^{(4)}(t)$ represents a time series of innovations, i.e., components of the data that cannot be explained from the dynamics itself. It is the aim of modelling to find dynamical models that produce a Gaussian white innovation time series, such that the process of modelling can be regarded as "temporal whitening".

where $A = I_{N_j}$. (67)

The parameter matrix A is of size $N_j \times N_j$, which is of the order of 10^8. This large number of parameters is still far too high to be estimated from real data; therefore we need additional reductions of model complexity. Also, the practical application of Kalman filtering requires a simplified model structure.

The term $\hat{j}^{(4)}(v,t-1/t-1)$ denotes the estimate of local current vector at voxal v at time $t-1$, i.e., the local state estimate, and $\rho(v,t-1/t-1)$ the corresponding estimate of the local error covariance matrix (3×3). For each voxal, the state prediction is given as

$$\hat{j}^{(4)}(v,t/t-1) = A\hat{j}(v,t-1/t-1) + \eta^{(4)}(t) \quad (68)$$

and the corresponding local prediction error covariance matrix can be approximated by

$$\rho(v,t/t-1) = A\rho(v,t-1/t-1)A^T + \sigma_\eta^2 I_3 \quad (69)$$

Innovation is described by

$$\Delta\vec{Y}(t) = \vec{Y}^{(4)}(t) - G^{(4)}\hat{J}^{(4)}(t/t-1) \quad (70)$$

$$\hat{j}^{(4)}(v,t/t-1) = \hat{j}^{(4)}(v,t-1/t-1) + K\Delta\vec{Y}(t) \quad (71)$$

The corresponding observation prediction error covariance matrix can be approximated by

$$R(t/t-1) = \sum_{v=1}^{N_v} G^{(4)}\rho(v,t/t-1)(G^{(4)})^T + C_\varepsilon \quad (72)$$

$$C_\varepsilon = \sigma_\varepsilon^2 I_{N_c} \quad (73)$$

The Kalman gain matrix for voxel v follows as

$$K = \rho(v,t/t-1)(G^{(4)})^T R(t/t-1)^{-1} \quad (74)$$

and

$$\rho(v,t/t) = (I_3 - KG^{(4)})\rho(v,t/t-1) \quad (75)$$

The term I is the identity matrix with dimensions $N_j \times N_j$.

II. Spike detection

The peaks from the output of filter, which are higher than threshold, are considered as an indication of the existence of an ES at that location in the time series. The absolute value of the estimated EEG is used for comparison with threshold. In spike detection,

the threshold is optimized to minimize missing of true peaks, while keeping the number of falsely detected peaks within a reasonable limit. The threshold is taken as scaled version of the mean of the absolute value of the estimated data in the whole signal duration. This modification makes the detection algorithm robust. Therefore, the threshold value for the KF-based approach is chosen as

$$T = \lambda \frac{1}{N} \sum_{t=1}^{N} z(x_t) \tag{76}$$

where N is the number of samples, λ is a scaling factor and $z(x_t)$ is the absolute value of the estimated data.

EEG Artifacts

A. Baseline wander

The baseline wander is an extraneous, low-frequency activity in the EEG, which may interfere with the signal analysis, making the clinical interpretation inaccurate. When baseline wander takes place, EEG measurements related to the isoelectric line cannot be computed, since it is not well-defined. Baseline wander is often exercise-induced and may have its origin in a variety of sources, including perspiration, respiration, body movements and poor electrode contact. The spectral content of the baseline wander is usually in the range between 0.05-1Hz, but during strenuous exercise, it may contain higher frequencies.

B. Power line interference

In many situations, the recorded signal is corrupted by different types of noise and interference, originated by another physiological process of the body. When an electrode is poorly attached to the body surface or when an external source such as the sinusoidal 50Hz power-line interferes with the signal, the recorded signal is distorted in a way that it could be difficult to perform any automatic diagnosis. The most external interferences associated with bioelectric signals are originated from the power line source. Such additive disturbances are usually modelled by: (1) a fixed frequency sinusoidal with random phase and amplitude (electrical field interference), and (2) higher order harmonics due to magnetic fields originated from nonlinear characteristics of the propagation path (e.g. main power transformer) due to other equipments like fluorescent lamp reactors.

C. Electromyographic (EMG) or Muscle Activity, Electrooculogram (EOG) and Electrocardiogram (ECG)

The artifacts in electroencephalogram records are caused by various factors, like line interference, Electromyographic (EMG) or Muscle Activity, EOG (electro-oculogram) and ECG (electrocardiogram). The EEG records carry information about abnormalities or responses to certain stimuli in the human brain. Some of the characteristics of these signals are the frequency and the morphology of their waves. These components are in the order of just a few up to 200 μV, and their frequency content differs among the different neurological rhythms, as the alpha, beta, delta and theta rhythms. Such rhythms are analyzed by physicians in order to detect neural disorders and cerebral pathologies. However, these rhythms are generally mixed with other biological signals, for example alpha is commonly mixed with the EOG (electro-oculogram). In this case, opening, closing or movements of the eyes produce artifacts in the EEG. The electrocardiogram (ECG) describes the electrical activity of the heart. It is obtained by placing electrodes on the chest, arms and legs. With every heartbeat, an impulse travels through the heart, which determines its rhythm & rate, and it causes the heart muscle to contract and pump blood. The voltage variations measured by the electrodes are caused by the action potentials of the excitable cardiac cells, as they make the cells contract. The ECG is characterized by a series of waves, whose morphology and timing provide information used for diagnosing diseases reflected by disturbances of the electrical activity of the heart. The time pattern that characterizes the occurrence of successive heartbeats is also very important.

D. Artifact drawbacks

The presence of artifacts in electroencephalogram records increases the difficulty in analysing the EEG and in obtaining clinical information. The artifacts introduce spikes, which can be confused with neurological rhythms. Thus, noise and undesirable signals must be eliminated or attenuated from the EEG to ensure a correct analysis and diagnosis.

E. Artifact excision technique

In the first step, the baseline wander, whose frequency is less than 1.0 Hz, is simply removed by high pass filtering. The baseline wander is also removed by a filter composed of a moving window centered at the sample under process. The signals obtained after the application of this window to the scalp, the EEG signal is subtracted from the original signal removing low frequency artifacts.

Several techniques have been developed to suppress power line interference (60 Hz or 50 Hz) and its higher harmonics from bioelectric signals. The physical solutions such as shielding, grounding and careful amplifier printed circuit board design are usually employed. Typically, such solutions are insufficient to provide the required signal quality level. The conventional low-pass analog filtering tends to severely attenuate signal components above its cut off frequency, which limits the system's frequency range. Such a limitation cannot be tolerated in applications, such as high-resolution electrocardiography. Different filtering solutions have been used for the removal of power line interference from EEG signal. Digital filter has been selected to overcome this problem, which can be divided into following categories.

- Low Pass Filters
- General Notch-Rejection Filters
- Adaptive Filters
- Global filters

The removal of power line interference from EEG signal can be removed by adaptive filtering, while the harmonics and high frequency noise can be removed by implementing general notch rejection filters. A notch filter is used to remove power line noise with a cut-off frequency of 60Hz in USA (or 50Hz in Europe and Asia). However, by this method brain activities with the same frequency are also removed out. Adaptive filtering is an alternative solution to power line interference cancellation. The adaptive noise canceller (ANC) developed by Widrow (Widrow et al., 1975) has been shown to lead to significant interference suppression in bioelectric signals. Its high selectivity, frequency tracking capability, low distortion and low computational cost characteristics are very attractive for bioelectric acquisition systems. Many modern commercial systems incorporate adaptive (active) noise cancelling

or techniques. Despite its excellent performance in 60 Hz (50 Hz) cancellation, the linear filtering structure of the ANC leads to a poor performance, when higher harmonics cancellation is necessary. For the suppression of power line harmonic in biomedical signals, a new technique proposes in (Marcio et al., 2009) is very effective and low computational cost strategy. In this technique, the power line reference is obtained from analog to digital conversion, while higher harmonics are mathematically estimated through trigonometric relations. These samples and estimates make up a set of reference signals to be processed by a multi-channel LMS adaptive canceller. The performance comparison with the conventional adaptive canceller in ECG and EEG demonstrates the new algorithm that can improve the signal to interference ratio of such bioelectric signals due to suppression of power line and harmonic interference.

To overcome EMG and EOG problems, many regression-based techniques have been proposed, including simple time domain regression (Croft and Barry, 2000) and frequency domain (Dimitris and Manolakis, 2000). The regression methods need calibration trials for determining the transfer coefficients between EOG, EMG and each of the EEG channels; they are not suitable for real time implementation. The real time artifacts removal is implemented by multi-channel Least Mean Square algorithm (Saeid et al., 2007). In this method horizontal EOG (HEOG), vertical (VEOG), and EMG signals are used as three reference digital filter inputs.

A recurrent neural network (RNNs) (Erfanian et al., 2005) was employed for modelling the interference signals. The RNNs are biologically more and computationally more powerful than feed-forward networks and their use is very appropriate for modelling nonlinear dynamic systems. The eye movement and eye blink artifacts were recorded by the placing of an electrode on the forehead above the left eye and an electrode on the left temple. The reference signal was then generated by the data collected from the forehead electrode being added to data recorded from the temple electrode. The reference signal was also contaminated by the EEG. To reduce the EEG interference, the reference signal was first low-pass filtered by a moving averaged filter and then applied to the ANC. Matlab Simulink was used for real-time data acquisition, filtering and ocular artifact suppression. Simulation results show the validity and effectiveness of the technique with different signal-to-noise ratios (SNRs) of the primary signal. On average, a significant improvement in SNR up to 27 dB was achieved with the recurrent neural network. The results from real data demonstrate that the proposed scheme removes ocular artifacts from the contaminated EEG signals and scheme is suitable for real-time and short-time EEG recordings. A digital signal processing technique like Independent Component Analysis (ICA) is used to remove the artifacts and interferences (Hu et al., 2004; Zhou et al., 2005).

A new automatic modified ICA approach (Devuyst et al., 2008) is used to eliminate ECG noise in an electroencephalogram or EOG. It is based on a modification of the ICA algorithm which gives promising results while using only a single-channel electroencephalogram (or electrooculogram) and the ECG. To check the effectiveness of approach, it is compared with other methods, that is, ensemble average subtraction (EAS) and adaptive filtering (AF). In the EAS method (Pander, 2004; Nakamura and Shibasaki, 2006; Dhiman et al., 2010), an average ECG-artifact waveform was computed for each homogeneous EEG portion, and an estimate of the artifact was generated by repeating this template synchronously with the interference peaks. This signal was then subtracted from the contaminated EEG to correct it. The adaptive filtering (AF) by using an ECG channel is introduced in (Sahul et al., 1995) for artifact cancellation. (Strobach et al., 1994) showed that this method was not appropriate if the ECG and the real interference exhibit remarkably deferent waveforms. They introduced a two-pass adaptive filtering algorithm, where an artificial reference was first generated by ensemble averaging related to the real interference than the ECG. Tests were carried out on simulated data obtained by addition of a filtered ECG on a visually clean original EEG and on real data made up of 10 excerpts of polysomnographic (PSG) sleep recordings containing ECG artifacts and other typical artifacts (e.g., movement, sweat, respiration, etc.).

A butterworth filter of order 10 with cut-off frequency of 45 Hz is used in (corsini et al., 2006). The conventional filtering cannot be applied to eliminate these types of artifacts because EEG signal and artifacts have overlapping spectra. To decrease such artifacts in EEG records, a cascade of three adaptive filters based on a least mean squares (LMS) algorithm is used. The adaptive filters are based on the optimization theory. The first one eliminates line interference, the second adaptive filter removes the ECG artifacts and the last one cancels EOG spikes. Each stage uses a finite impulse response (FIR) filter, which adjusts its coefficients to produce an output similar to the artifacts present in the EEG. The cascade adaptive filter was tested in five simulated EEG records. In all cases, line-frequency, ECG and EOG artifacts were attenuated. An adaptive filter reduces the common artifacts present in EEG signals without removing significant information embedded in these records. The objective of an adaptive filter is to change (adapt) the coefficients of the linear filter, and hence its frequency response, to generate a signal similar to the noise present in the signal to be filtered. The adaptive process involves minimization of a cost function, which is used to determine the filter coefficients. By and large, the adaptive filter adjusts its coefficients to minimize the squared error between its output and a primary signal. In stationary conditions, the filter should converge to the Wiener solution. The advantages of using a cascade of three filters instead of filtering the three signals with a single adaptive filter are among others,

- The coefficient's adaptation in three independent filters is simpler and faster than their adaptation in a single filter.
- At each stage output, the error signals, EEG with one of the three attenuated artifacts are present; such separation (by artifact) may be useful in some applications, where such output might be enough.

The advantages of adaptive filters over conventional ones include preservation of components intrinsic to the EEG record. Besides, they can adapt their coefficients to variations in heart frequency, abrupt changes in the line frequency (caused, say, by ignition of electric devices) or modifications due to eye movements.

A difficulty found in this work was the determination of L (filter order) and μ (convergence factor). These parameters are very important; L, because it leads to appropriate filtering, and μ, to get adequate adaptation. If μ is too big, the filter becomes unstable, and if it is too small, the adaptation may turn out too slow. Several

tests were carried out to determine the optimum value for these parameters.

Concluding Remarks & Future Scope

In EEG source analysis, the inverse problem estimates the sources within the brain giving rise to a scalp potential recording. The KF model based an estimation technique is well suited to solve inverse problem. In the inverse problem, an EEG source can be reconstructed using linear and nonlinear physiological based dynamic models with time varying parameters and Kalman filter. Using Kalman filter the current densities and parameters of the model can be estimated simultaneously. The inverse problem is formulated for linear and nonlinear dynamics compact Physiological model as follows

$$\vec{Y}^{(5)}(t) = \vec{G}^{(5)}\vec{J}^{(5)}(s,t) + \vec{\varepsilon}^{(5)}(t) \tag{77}$$

Eq. (77) is the ill posed problem and the estimation $\hat{J}^{(5)}(t)$ of $J^{(5)}(t)$ can be obtained by minimizing the objective function given in Eq. (78) for each time t independently

$$E[J^{(5)}(t)] = \left\|Y^{(5)}(t) - G^{(5)}J^{(5)}(t)\right\|^2_{C_\varepsilon} + \lambda^2\left\|LJ^{(5)}(t)\right\|^2 \tag{78}$$

where L is a matrix with $3N \times 3N$ dimensions. It is obtained by spatial smoothness constraints, where the i^{th} source vector of L acts as discrete differentiating operator (Laplacian operator), by forming the difference between the nearest neighbours of the j^{th} source itself. λ is the regularization parameter which balances between fitting the model and prior constraint of minimizing $\left\|LJ^{(5)}(t)\right\|$. An estimate $\hat{J}^{(5)}(t)$ can be obtained by minimizing the Eq. (78).

$$\hat{J}^{(5)}(t) = \arg\cdot\min_{J(k)}\{\left\|Y^{(5)}(t) - GJ^{(5)}(t)\right\|^2_{C_\varepsilon{}^{(5)}} + \lambda^2\left\|LJ^{(5)}(t)\right\|^2\} \tag{79}$$

The dynamic inverse problem sustains the same equation for the measurement of observations, but taken into account the dynamics of current densities $J^{(5)}(t)$. This problem can be formulated for the linear dynamics compact Physiological model as follows

$$J^{(5)}(t) = f[J^{(5)}(t-1), J^{(5)}(t-2)] + \eta^{(5)}(t) \tag{80}$$

where f is a vectorial function that takes into the dynamics of the current density and $\eta^{(5)}{}_G(t) = \tau^2 C_\eta$. In which $C_{\eta^{(5)}} = (L^T L)^{-1}$ is covariance matrix associated with η. In case of discretized linear model, (80) is defined in (81). The global process model as a second-order multivariate AR model

$$J^{(5)}(t) = A^{(5)}_{G1}J^{(5)}(t-1) + A^{(5)}_{G2}J^{(5)}(t-2) + \eta^{(5)}_G(t) \tag{81}$$

where the $N_{J^{(5)}} \times N_{J^{(5)}}$ global parameter matrices are

$$A^{(5)}_{G1} = a_1 I_{NJ^{(3)}} + b_1 L; A^{(5)}_{G2} = a_2 I_{NJ^{(3)}} \tag{82}$$

The $N_{J^{(5)}}$ -dimensional vector $\eta^{(5)}_G(t)$ is a dynamical noise term that is assumed white, Gaussian, and unbiased, with covariance matrix $C_{\eta^{(5)}_G}$. In which $A^{(5)}_{G1}$ & $A^{(5)}_{G2}$ are matrix of $3N \times 3N$. The structure of $A^{(5)}_{G1}$ & $A^{(5)}_{G2}$ are selected according to spatiotemporal physiological model. In which, a_1 considers the variability among sources in time and b_1 in space.

Equation (81) can be reformulated in the form of first order model as

$$\begin{bmatrix} J^{(5)}(t) \\ J^{(5)}(t-1) \end{bmatrix} = \begin{bmatrix} A^{(5)}_{G1} & A^{(5)}_{G2} \\ I & 0 \end{bmatrix}\begin{bmatrix} J^{(5)}(t-1) \\ J^{(5)}(t-2) \end{bmatrix} + \begin{bmatrix} I \\ 0 \end{bmatrix}\eta^{(5)}_G(t) \tag{83}$$

This problem can be formulated for the nonlinear dynamics compact Physiological model as follows

$$J^{(5)}(t) = A^{(5)}_{G1}[J^{(5)}(t-1)] + A^{(5)}_{G2}[J^{(5)}(t-1)]^2 + A^{(5)}_{G3}[J^{(5)}(t-1)]^3 + A^{(5)}_{G4}[J^{(5)}(t-2)] + \eta^{(5)}_G(t) \tag{84}$$

where

$$A^{(5)}_{G1} = a_1 I_{NJ} + b_1 L; A^{(5)}_{G2} = a_2 I_{NJ} \tag{85}$$

$$A^{(5)}_{G3} = a_3 I_{NJ}; A^{(5)}_{G4} = a_4 I_{NG} \tag{86}$$

Similarly, an ill posed dynamic inverse problem for nonlinear dynamics compact Physiological model can be solved by minimizing the following objective function

$$E[J^{(5)}(t)] = \left\|Y^{(5)}(t) - G^{(5)}J^{(5)}(t)\right\|^2_{C_\varepsilon} + \lambda^2\left\|J^{(5)}(t) - f[J^{(5)}(t-1), J^{(5)}(t-2)]\right\|^2_{\eta^{(5)}} \tag{87}$$

The initial estimate for $(t=1)$ of the state $J^{(5)}(1)$ can be obtained by any approach for solving the inverse problem. For $k = 2,...,N_k$, where N_k is the total number of samples, we can obtain $\hat{J}^{(5)}(t)$ by minimizing (87). For the solution of linear and non-linear models, two sequence Kalman filter and two sequence extended Kalman filter in (87) are used for neural activity estimation and parameter estimation.

The Kalman filter approach uses the temporal information and the time varying nature of EEG component to detect the ESs. In the

presence of noise, the detection of ESs in EEG is difficult because of the wide variation of the ESs characteristics. The independent component analysis (ICA) is used to remove the artifacts and interferences. Three adaptive filters in cascade, based on LMS algorithm, are used in order to cancel common artifacts (line interference, ECG and EOG) present in EEG records. The EEG forward problem estimates field matrix without considering the artifacts. In EEG source analysis, the inverse problem estimates the sources within the brain giving rise to a scalp potential recording without considering the artifacts. Artifacts can be introduced for the calculation of forward and inverse problem.

However, despite the large body of literature on "*Neural Signal Processing Paradigms*", the current knowledge on the "*Physiological Models for EEG*" is probably still only the tip of the iceberg.

References

[1] Ary J.P.Z., Klein S.A., Fender D.H. (1981) *IEEE Transactions on Biomedical Engineering*, 28, 447-452.

[2] Barton M., Robinson P., Kumar S., Galka A., Durrant-White H., Guivant J., Ozaki T. (2009) *IEEE Transactions on biomedical Engineering*, 56(1), 122-136.

[3] Carlos Guerrero-Mosquera and Angel Navia Vazquez (2009) 31*th Annual International Conference of the IEEE EMBS*, 13-16.

[4] Corsini Javier, Shoker Leor, Sanei Saeid (2006) *IEEE Transactions on Biomedical Engineering*, 53(5).

[5] Croft R.J., Barry R.J. (2000) *Neurophysiologie Clinique*, 30, 5-19.

[6] Daunizeau Jean, Mattout Jeremie, Clonda Diego, Goulard Bernard, Benali Habib, Lina Jean-Marc (2006) *IEEE Transactions on Biomedical Engineering*, 53(3), 503-516.

[7] Devuyst Stephanie, Dutoit Thierry, Stenuit Patricia, Kerkhofs Myriam, Stanus Etienne (2008) *EURASIP Journal on Advances in Signal Processing*.

[8] Dhiman Rohtash, Saini J.S., Priyanka, Mittal A.P. (2010) *National Conference on Computational Instrumentation CSIO,* 62 -66.

[9] Dimitris G., Manolakis (2000) *Statistical and adaptive signal processing. MC Graw Hill, Clinique*, 30, 5-19.

[10] Ellenrieder Nicolas Von, Muravehik Carlos H., Nehorai Arye (2006) *IEEE Transaction on Biomedical Engineering*, 53(3), 421-429.

[11] Erfanian A., Mahmoudi B. (2005) *Medical & Biological Engineering & Computing*, 43.

[12] Feige Bernd, Scheffler Klaus, Esposito Fabrizio, Salle Francesco Di, Hennig Jurgen, Seifritz Erich (2005) *J Neurophysiol,* 93, 2864-2872.

[13] Galka Andreas, Ozaki Tohru, Muhle Hiltrud, Stephani Ulrich, Siniatchkin Michael (2008) *A data-driven model of the generation of human EEG based on a spatially distributed stochastic wave equation.* 2, 101-113.

[14] Galka A., Yamashita O., Ozaki T., Biscay R., Valde´s-Sosa P. A. (2004) *NeuroImage*, 23, 435-453.

[15] Galka A., Yamashita O., Ozaki T. (2004b) *Phys Lett A*, 333, 261-268.

[16] Giraldo E., Dekker A.J. den, Castellanos-Dominguez G. (2010) 32*nd Annual International Conference of the IEEE EMBS*, 2914-2917.

[17] Grech R., Tracey C., Muscat J., Camilleri K., Fabri S., Zervakis M., Xanthoupoulos P., Sakkalis V., Vanrumste B. (2008) *Journal of NeuroEngineering and Rehabilitation*, 5(25)

[18] Harke K.C., Schlogl A., Anderer P., Pfurtscheller G. (1999) *European Medical and Biological Engineering Conference*, 482-483.

[19] Hu Sanqing, Stead Matt, Worrell Gregory A. (2007) *NIH*, 1486 -1491.

[20] Ji Zhanfeng, Sugi Takenao, Goto Satoru, Wang Xingyu (2011) *International Conference on Complex Medical Engineering,* 179-184.

[21] Katrina Wendel, Kalervo Suominen, Pasi Kauppinen, Eila Sonkajarvi, Jarno M.A. Tanskanen, Kotoe Kamata, Outi Vaisanen, Jari Hyttinen, and Ville Jantti (2011) *NFSI & ICBEN, IEEE*, 126-130.

[22] Ko Cheng-Wen, Chung Hsiao-Wen (2000) *Clinical Neurophysiology,* 111, 477-481.

[23] Mahmoud El-Gohary, James McNames, and Siegward Elsas (2008) 30*th Annual International IEEE EMBS Conference*, 821 -824.

[24] Marcio H. Costaa, Mauricio C. Tavares (2009) *Computers in Biology and Medicine, Elsevier,* 39(15), 519 - 526.

[25] Masherov E.L., Volynsky P.E., Shekut'ev G.A. (2009) *Human Physiology*, 35(4), 502-512.

[26] Mneimneh M.A., Yaz E.E., Johnson M.T., Povinelli R.J. (2006) *Computers in Cardiology*, 33, 253-256.

[27] Mousavi S. R., Niknazar M., Vahdat B. Vosougi (2008) *IEEE, CIBEC*.

[28] Nakamura M., Shibasaki H. (1987) *Electroencephalography and Clinical Neurophysiology,* 66(1), 89-92.

[29] Noureddin Borna, Lawrence Peter D., Rich Gary E. (2009) *Conference on Neural Engineering IEEE EMBS*, 614-617.

[30] Nunez P.L. (1981) *Electrical fields of the brain. Oxford University Press, New York*.

[31] Nunez P.L., Srinivasan R. (2006) *Electric fields of the brain. The Neurophysics of EEG*, 2*nd ed*.

[32] Pander T.P. (2004) 26*th Annual International Conference of the IEEE EMBS*, pp. 596-99.

[33] Park H.J., Jeong D.U., Park K.S. (2002) *IEEE Transactions on Biomedical Engineering*, 49(12),2, 1526-1533.

[34] Pascual-Marqui RD, Michel CM, Lehmann D (1994) *Int J Psychophysiol*, 18, 49-65.

[35] Riera J.J., Fuentes M.E., Valde´s P.A., Oha´rriz Y. (1998) *Inverse Probl*, 14, 1009-1019.

[36] Robinson P., Kim, J. (2007) *Physical Review E*, 75(1), 0319071-03190710.

[37] Robinson P.A., Rennie C.J., Rowe D.L., O'Connor S.C. (2004) *Human Brain Mapping*, 72, 23-53.

[38] Robinson P.A., Rennie C.J., Wright J.J. (1997) *The American Physical Society*, 56(1), 826-840.

[39] Romero Sergio, Mananas Miguel Angle, Barbanoj Manuel Jose (2009) *Annual International Conference of the IEEE EMBS*, 5495-98.

[40]Ryynanen Outi R.M., Hyttinen Jari A.K., Laarne Paivi H. (2004) *IEEE Transaction on Biomedical Engineering*, 51(9), 1547-54.
[41]Ryynanen Outi R. M., Hyttinen Jari A. K., Malmirvuo A. (2006) *IEEE Transaction on Biomedical Engineering*, 53(9), 1851-58.
[42]Saeid Mehrkanoon, Mahmoud Moghavvemi, Hossein Fariborzi (2007) *International Conference on Intelligent and Advanced Systems*, 1245-1250.
[43]Sahul Z., Black J., Widrow B., Guilleminault C. (1995) *Sleep Research*, 24(A), 486.
[44]Shahid Shahjahan, Walker Jacqueline, Smith Leslie S. (2010) *IEEE Transactions on Biomedical Engineering*, 57(4), 853-866.
[45]Sheeba Jane H., Stefanovska Aneta, McClintock Peter V. E. (2008) *Biophysical Journal* 95, 2722-2727.
[46]Strobach P., Abraham-Fuchs K., Harer W. (1994) *IEEE Transactions on Biomedical Engineering*, 41(4), 343-350.
[47]Tarvainen M.P., Ranta-aho P.O., Karjalainen P.A. (2001) 23*rd Annual Conference - IEEE/EMBS*.
[48]Tian X., Xiao Z.G. (2005) *First International Conference on Neural Interface and Control*, 217-220.
[49]Vatta Federica, Mneghini Fabio, Esposito Fabrizio, Minine Stefanol, Vatta Francesco Di Salle Federica, Meneghini Fabio (2010) *Computational Intelligence and Neuroscience*.
[50]Wallingford Errol E., Collins W.R. (1978) *IEEE Transaction on Insrumentation and Measurement*, 27(1).
[51]Widrow B., Glover Jr. J.R., McCool J.M., et al. (1975) *IEEE* 63 (12), 1692-1716.
[52]Yamashita O, Galka A, Ozaki T, Biscay R, Valde´s-Sosa PA (2004) *Hum Brain Map*, 21, 221-235.
[53]Ye Yuan, Yue Li, Dongyan Yu, Danilo P. Mandic (2008) *IEEE*, pp. 502-505.
[54]Zhou Weidong, Zhou Jin, Zhao Hao, Ju Liu (2005) *Engineering in Medicine and Biology 27th Annual Conference of IEEE,* 6017-6020.

About Authors

Harish Kumar Garg is presently pursuing Ph.D. in Electronics and Communication Engineering Department of Thapar University Patiala, Punjab, India. His research interests include neural networks, bio-medical engineering, and adaptive system design. He is author as well as reviewer of various research papers published in the distinguished international journals.

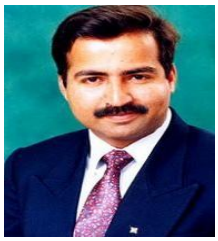

Amit Kumar Kohli received the B.Tech. (Honor) degree from Guru Nanak Dev Engineering College, Ludhiana, the M.E. (Highest Honor) degree from Thapar University Patiala (previously Thapar Institute of Engineering and Technology) and the Ph.D. degree from Indian Institute of Technology, Roorkee, India, in 2000, 2002 and 2006 respectively, all in electronics and communication engineering.

He is presently Senior Assistant Professor in Electronics and Communication Engineering Department of Thapar University Patiala, India. His research interests include signal processing and its applications, modeling of fading dispersive channels, wireless & high data rate advanced communication systems, neural networks & bio-medical engineering and adaptive system design. He is author as well as reviewer of various research papers published in the distinguished international journals/transactions of IEEE, Springer, Taylor & Francis and Elsevier etc. He received National Scholarship, State Scholarship, MHRD Fellowship, Institution Medal, and Gold Medal consecutively for academic performance.

Poonam G. Kohli received the M.B.B.S. degree from Government Medical College & Hospital Amritsar, Baba Farid University of Health Sciences Punjab and the M.D. (Physiology) degree from Government Medical College & Hospital Patiala, Baba Farid University of Health Sciences Punjab, India, in 2004 and 2009 respectively. She is presently Assistant Professor in the Physiology Department of Punjab Institute of Medical Science, Jalandhar, India. Her research interests include physiological studies and application of bio-medical engineering in the emerging fields of medical science. She received Punjab State Government Scholarship/Fellowship through out her M.D. degree.